Probing the Early Events Associated with Liquid Ammonia Pretreatment of Native Crystalline Cellulose

ARTICLE *in* THE JOURNAL OF PHYSICAL CHEMISTRY B · AUGUST 2011

Impact Factor: 3.3 · DOI: 10.1021/jp2048844 · Source: PubMed

5 AUTHORS, INCLUDING:

Giovanni Bellesia
University of California, Santa Barbara
26 PUBLICATIONS **568** CITATIONS
SEE PROFILE

Shishir Chundawat
Rutgers, The State University of New Jersey
66 PUBLICATIONS **2,079** CITATIONS
SEE PROFILE

Paul Langan
Oak Ridge National Laboratory
123 PUBLICATIONS **3,058** CITATIONS
SEE PROFILE

Bruce E Dale
Michigan State University
333 PUBLICATIONS **11,025** CITATIONS
SEE PROFILE

THE JOURNAL OF PHYSICAL CHEMISTRY B

ARTICLE

pubs.acs.org/JPCB

Probing the Early Events Associated with Liquid Ammonia Pretreatment of Native Crystalline Cellulose

Giovanni Bellesia,[†] Shishir P. S. Chundawat,[‡,⊥] Paul Langan,[§,▽] Bruce E. Dale,[‡,⊥] and S. Gnanakaran*[,∥]

[†]T6 & CNLS, Los Alamos National Laboratory, Los Alamos, New Mexico 87545, United States

[‡]Biomass Conversion Research Laboratory, Department of Chemical Engineering and Material Science,Michigan State University, Lansing, Michigan 48824, United States

[§]Bioscience Division, Los Alamos National Laboratory, Los Alamos, New Mexico 87545, United States

[∥]T6, Los Alamos National Laboratory, Los Alamos,New Mexico 87545, United States

[⊥]DOE Great Lakes Bioenergy Research Center, East Lansing, Michigan 48824, United States

Supporting Information

ABSTRACT: Various chemicals are being explored for catalyzing efficient lignocellulose deconstruction. In particular, when liquid ammonia is used to convert the naturally occurring cellulose crystalline phase I_β, to cellulose III_I, the rearrangement of the hydrogen bond network in cellulose III_I results in enhanced hydrolysis yields. We use molecular dynamics simulations to analyze the interaction between a cellulose I_β fibril and ammonia. Our simulations reveal that early structural changes in the fibril are driven by the rapid formation of an extended hydrogen bond network between the solvent-exposed surface chains and ammonia that precedes ammonia penetration into the fibril. The emergence of this hydrogen bond network causes relative shifting of the cellulose layers within the fibril that in turn leads to the formation of channels orthogonal to the (100) and (−100) fibril surfaces. The channels allow ammonia molecules to penetrate into the cellulose fibril. These findings provide avenues for improving existing chemical pretreatments to make them more effective and economical.

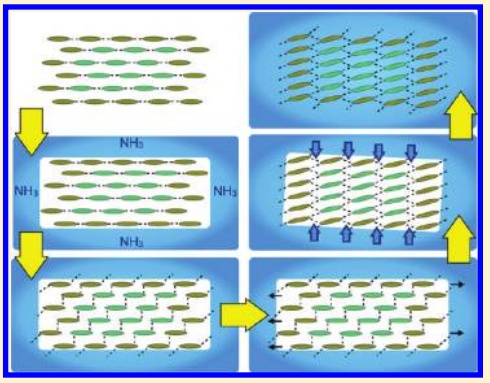

INTRODUCTION

Cellulose, a linear polymer composed of $\beta(1-4)$ linked D-glucose units and a major component of lignocellulosic biomass, is synthesized at the plasma membrane of growing plants from arrays of cellulose synthase complexes[1] as crystalline nanofibers whose unit cell parameters and space group are identified as cellulose I_β. In a typical process of biomass conversion for biofuels production, thermochemical pretreatments are, first, used to improve enzyme accessibility of cellulose fibers which, in untreated biomass, are embedded in an amorphous matrix of hemicellulose and lignin. Then cellulose is hydrolyzed by enzymes to glucose that can eventually be converted to biofuels via microbial fermentation or chemical catalysis.[2,3] However, intracrystalline hydrogen bonds and stacking interactions in cellulose I_β fibers make crystalline cellulose recalcitrant to enzymatic hydrolysis, therefore hindering the efficiency of the cellulose-to-glucose conversion process.[2−4]

One route to improve cellulose hydrolysis relies on the use of liquid ammonia to catalyze a structural crossover from cellulose I_β to another crystalline cellulose allomorph named cellulose III_I. This structural crossover leads to rearrangement of both the intracrystalline hydrogen bonds and the stacking interactions between the glucose rings.[5,6] Recent experiments have shown that such a rearrangement in cellulose III_I enhances the enzymatic hydrolysis rates by up to 5-fold with respect to cellulose I_β.[7] In addition to the enhancement in cellulose digestibility, ammonia−based treatments (e.g., AFEX) have additional advantages over other pretreatment technologies in terms of both economic feasibility and environmental impact.[8] X-ray and neutron diffraction structures for cellulose I_β, cellulose III_I as well as for the transient ammonia−cellulose I complex are known.[6,9,10] The latter is an intermediate state where ammonia molecules are trapped in specific sites within the cellulose crystal and form hydrogen bonds with the neighboring cellulose chains.[10] Cellulose III_I is generated from the ammonia−cellulose I complex upon ammonia evaporation which prompts an alteration in the hydrogen bond network and a related relatively small rearrangement of the packed cellulose chains.[6,9,10] While the experimental protocol for the ammonia-based conversion from cellulose I_β to cellulose III_I is well established, the atomistic details of the structural crossover from cellulose I_β to the ammonia−cellulose I complex and to cellulose III_I are still unknown. In this study we use an extensive set of fully atomistic molecular dynamics (MD) simulations to analyze the

Received: May 25, 2011
Revised: June 30, 2011
Published: July 05, 2011

early stages of the interaction between liquid ammonia and a cellulose I_β fibril.

We observe a sequence of events characterizing the early stages of the interaction between liquid ammonia and native crystalline cellulose. These events can be summarized as follows: (I) Formation of hydrogen bonding network between the ammonia molecules in the vicinity of the cellulose fibril and the cellulose chains on the surface of the fibril. (II) Consequential change in the hydroxymethyl group rotational state population from *tg* (the rotational state observed in cellulose I_β) to *gt* and *gg* (the rotational states observed experimentally and in previous simulation studies, in the ammonia−cellulose I complex, in cellulose III_I as well as in amorphous and fully solvated cellulose). The change in the hydroxymethyl rotational state population appears to start from the cellulose chains exposed to the ammonia solvent and then quickly propagate to the core of the fibril. (III) Structural crossover from cellulose I_β to a new crystalline structure where the chain stacking arrangement in the plane perpendicular to the fibril main axis is similar to that observed in the ammonia−cellulose I complex and cellulose III_I. (IV) Ammonia penetration appears to follow major fibril structural changes, suggesting that liquid ammonia and its interaction with the cellulose surface is a prerequisite for structural changes required for the conversion from cellulose I_β to cellulose III_I.

MATERIALS AND METHODS

X-ray and neutron diffraction coordinates[5] were used to generate one "rhomboid" cellulose I_β fibril composed by 30 octameric glucan (cellulose) chains. All MD simulations were performed under NPT conditions (isothermal−isobaric ensemble), using the NAMD software,[11] with the GLYCAM06[12] force field. The following parametrization was used for the ammonia molecule:[13,14] $N_{charge} = -1.026e$, $H_{charge} = 0.342e$, $K_{bond} = 394.1$ kcal/mol, $r_0 = 1.018$ Å, $K_{angle} = 41.3$ kcal/mol, $\theta_0 = 107.13$ (deg), $A_{NN} = 9.44293233 \times 10^5$, $A_{NH} = 2.12601181 \times 10^3$, $A_{HH} = 1.39982777 \times 10^{-1}$, $B_{NN} = 8.01323529 \times 10^2$, $B_{NH} = 2.09604198 \times 10$, $B_{HH} = 9.37598976 \times 10^{-2}$. Units for the *A* and *B* Lennard-Jones coefficients are (kcal/mol) Å^{12} and (kcal/mol) Å^6, respectively. Results from a MD simulation of a liquid ammonia box show good agreement with both the experimental density and the experimental N−N radial distribution function (data not shown). Further validation of the ammonia model comes from a recent neutron diffraction and molecular dynamics study where both the structure and the dynamics of an ammonia−cellulose I infinite crystal were studied in detail.[10]

The fibril was solvated in a rectangular ammonia box, and each glucan chain was covalently connected to its periodic image along its main axis in order to mimic an infinitely long chain (fibril). A snapshot of the solvated cellulose I_β fibril is given at the top of Figure 1. The initial ammonia coordinates were obtained from an equilibrated box of liquid ammonia. A Langevin thermostat and a Nose−Hoover Langevin barostat[15,16] were used to control the temperature and the pressure, respectively. The damping coefficient for the Langevin integrator was set to $b = 1.0$ ps^{-1}, whereas for the Nose−Hoover Langevin barostat we applied an oscillation period of 200 fs and a damping period of 100 fs. The cutoff for the nonbonded interactions in the coordinate space was fixed at 10.0 Å. All of the simulations were performed under periodic boundary conditions, and the long−range electrostatic interactions were calculated by using the Ewald summation method with the particle mesh Ewald algorithm.[17] The particle mesh Ewald accuracy was fixed at 10^{-6}, the order of the interpolation functions on the grid was set to 4 (cubic), and the grid size was ∼1.0 Å. The time step was fixed in all simulations at 2.0 fs. The covalent bonds involving hydrogen atoms were constrained by means of the SHAKE algorithm.[18]

We considered more than 60 distinct MD simulations totaling 832 ns to capture nonequilibrium dynamics involving ammonia−cellulose interaction. The simulation set #1 was carried out to analyze the early changes in the hydroxymethyl group rotational state as well as the cellulose and cellulose−ammonia hydrogen bonds networks. Here, the initial conformation was generated performing, first, a local optimization followed by a short thermal relaxation of the liquid ammonia with the cellulose fibril atoms kept fixed. This initial conformation was used to start 40 independent NPT−MD simulations, 100 ps each. The pressure was fixed at $P = 1.01325$ bar, whereas two different temperatures were used (each for 20 MD simulations): $T = 298$ and 413 K.[9] The simulation set #2 was carried out to probe the onset of the "macroscopic" structural changes in the fibril (changes in the mutual distances of the glucan chains within the fibril) as well as the ammonia molecules "penetration" into the fibril. The initial conformation for this set of simulations was generated performing, first, a local optimization followed by a short (∼1.0 ns) NPT−MD simulation ($P = 1.01325$ bar), where the temperature was gradually increased from 100 to 298 K (no atoms were fixed). This initial conformation was used to start 20 independent NPT−MD simulations. Of these 20 simulations, 10 were 10 ns long with $T = 298$ K, and 10 were 50 ns long with $T = 413$ K. Additional MD simulations (set #3) on ammonia−solvated cellulose fibrils were performed at $T = 413$ K on both a cellulose I_β and a cellulose III_I fibril (76 and 62 ns, respectively), and at $T =$ 450, 550, and 650 K (set #4) on a cellulose I_β fibril (30 ns each). The temperature $T = 413$ K was chosen in accordance with the experimental temperature used by Wada et al. to obtain ammonia−cellulose I complex from native cellulose I_β.[9] Higher temperatures ($T = 450$, 550, and 650 K) were chosen in order to observe a more extensive ammonia penetration within reasonably short simulation time lengths.

Hydrogen bonds within the cellulose fibril and between cellulose and liquid ammonia were defined by a cutoff distance of 3.3 Å and a cutoff angle of 30°.[19−21] The values of the dihedral angles χ(O5−C5−O6−C6) and χ'(C4−C5−O6−C6) were employed to define the rotational state of the hydroxymethyl group. Three main rotational states were considered: (i) *tg* (trans−gauche), typically found in cellulose I_β,[5] (ii) *gt* (gauche−trans), dominant in cellulose III_I[6] and in the ammonia−cellulose I complex,[9] and also observed in both amorphous and solvated cellulose[22,23] and (iii) *gg* (gauche−gauche), observed in both amorphous and solvated cellulose.[22,23] The ammonia−induced structural changes were monitored via three parameters: the distances a' and b', and the angle γ', all defined in Figure S1. In the cellulose I_β structure, $a' = (a^2 + b^2 + 2ab\cos(\gamma))^{1/2}$ and $\gamma' = 180° - \arcsin(\sin(\gamma)a/(2a^*))$ where a, $b' = b$ and γ define the crystal unit in the plane perpendicular to the cellulose chain main axis,[5] and $a^* = 0.5(a^2 + b^2 - 2ab\cos(\gamma))^{1/2}$. In the ammonia−cellulose I complex and in the cellulose III_I structures, $a' = 2a$, $b' = b$ and $\gamma' = \gamma$.[6,9] In cellulose I_β (our starting configuration), $a' = 10.7$ Å and $\gamma' \sim 140°$. $a' = 8.9$ Å in both the ammonia−cellulose I complex and cellulose III_I while $\gamma' = 92.7°$ and $\gamma' = 105°$ in the ammonia−cellulose I complex and in cellulose III_I, respectively.

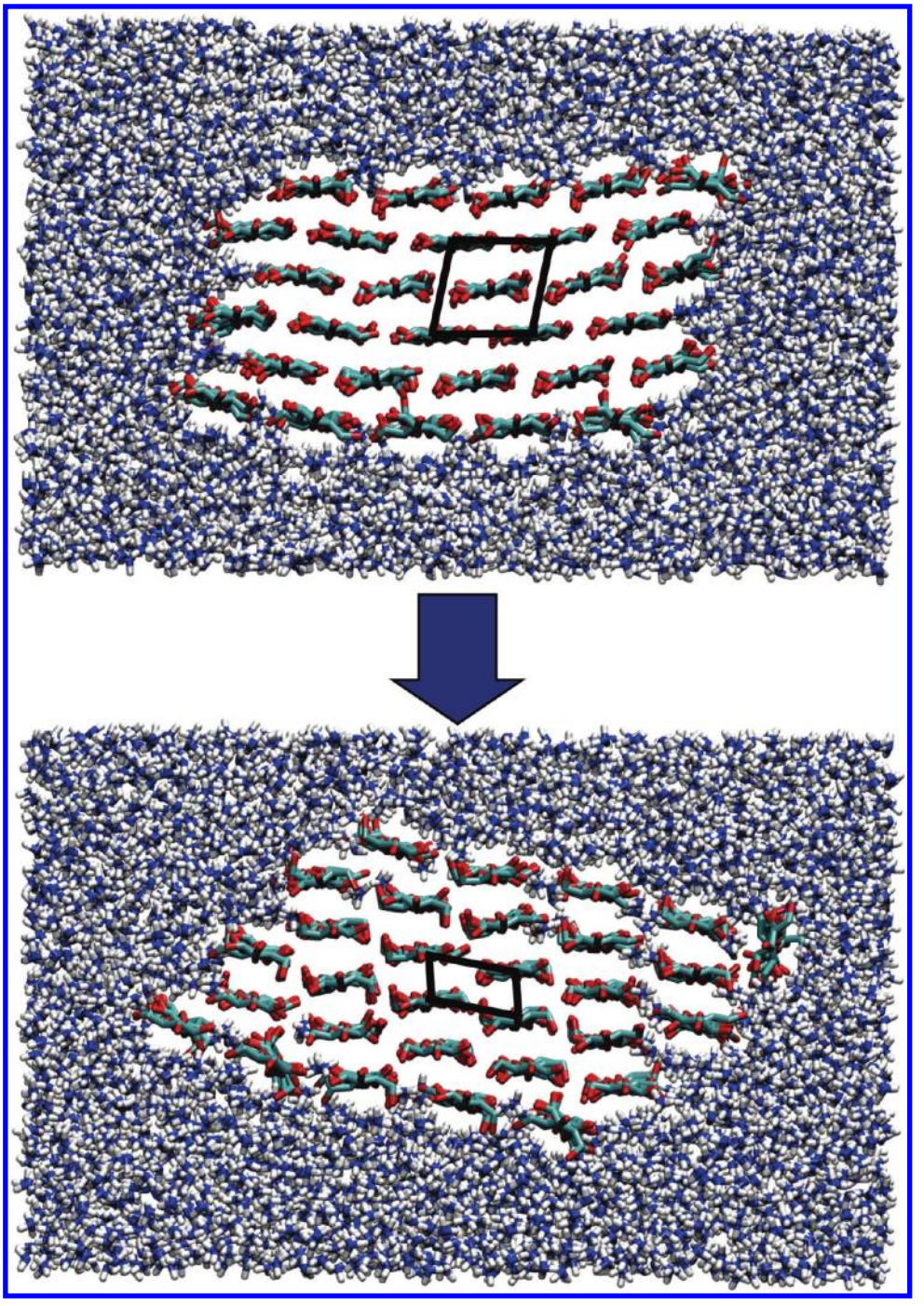

Figure 1. Top: starting configuration: ammonia−solvated cellulose I_β fibril. Bottom: cellulose fibril compatible with ammonia−cellulose I complex symmetry obtained after 76 ns at $T = 413$ K. Only partial ammonia penetration is observed. The black parallelograms indicate the respective crystal units in the $a-b$ plane.

RESULTS AND DISCUSSION

At very early time scales, we monitor rapid formation of hydrogen bonding between NH_3 and exposed chains of cellulose. The simulation set #1 that includes more than 40 separate simulations of 100 ps each was used to characterize these early events. At time $t = 0$, the "internal" cellulose hydrogen bond network was the one typical of cellulose I_β[5] and there were no hydrogen bonds between cellulose and the ammonia molecules. Then, in a few picoseconds, we observe a rapid increase in the number of hydrogen bonds between ammonia molecules and solvent-exposed cellulose chains. This new hydrogen bond network involves mainly backbone oxygen atoms O2 and O3 as well as side−chain oxygen atom O6 in the hydroxymethyl group. The time evolution for the number of cellulose−ammonia hydrogen bonds considering O6, O3, and O2 as both donors and acceptors, and O5 as acceptor at $T = 298$ K is shown in Figure 2. The hydrogen bonding network profile is slightly lower at higher temperature ($T = 413$ K, Figure S2 in the Supporting

dx.doi.org/10.1021/jp2048844 |J. Phys. Chem. B 2011, 115, 9782–9788

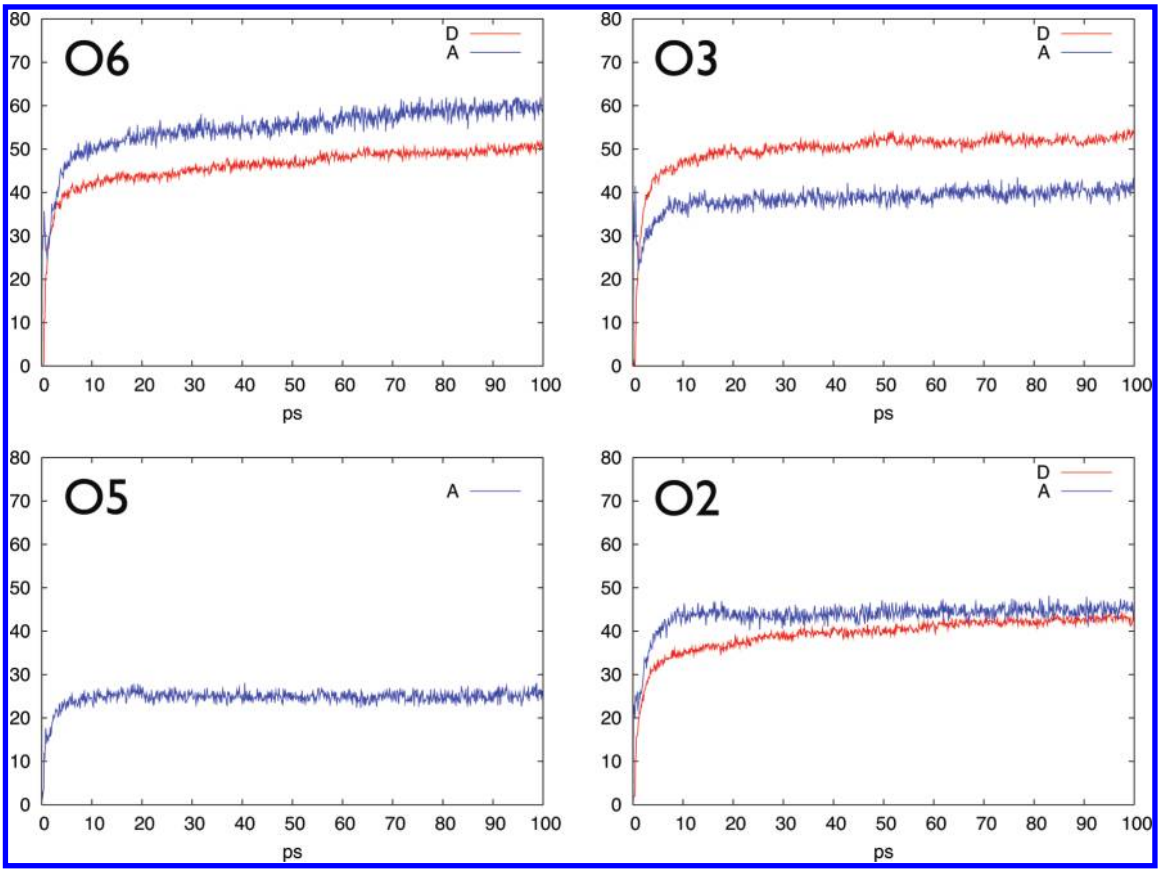

Figure 2. Early (100 ps) time evolution for the number of cellulose−ammonia hydrogen bonds, considering cellulose atoms O6, O3, and O2 as both donors (D, red) and acceptors (A, blue) and O5 as acceptor at T = 298 K. The plots are generated from values averaged over 20 trajectories. The errors vary between 0.5 and 1.5.

Information). The minor contribution of O4 as acceptor is not shown. The "internal" cellulose hydrogen bond network also undergoes substantial changes within the 100 ps MD simulation length, namely, the numbers of intrasheet hydrogen bonds (intra- and intermolecular) decrease while the number of intersheet hydrogen bonds increases[7] (Figure S3 in the Supporting Information).

The same set of simulations show a decrease in the hydroxymethyl group rotational state *tg* compensated by a corresponding increase in both *gt* and *gg* rotational states. At time t = 0, all of the hydroxymethyl groups in the cellulose fibril were in the *tg* state (tg_{fraction} = 1.0). The subsequent observed shift in rotational states appears to be a consequence of the rapid formation of hydrogen bonds between ammonia molecules and solvent−exposed cellulose chains. In Figure 3 we show representative plots of the time evolution (over t = 100 ps) of the *tg*, *gt*, and *gg* populations for solvent−exposed chains at T = 413 K and T = 298 K (A and B, respectively) as well as for cellulose chains in the crystalline core at T = 413 and 298 K (C and D, respectively). The decrease in the *tg* population is faster in the solvent−exposed chains than in the chains within the crystalline core of the fibril. The changes in the hydroxymethyl group rotational state occupancy are also generally faster at higher temperature (See Figure S4 in the Supporting Information).

Along much longer time scales, we observe global structural changes that affect the crystalline structure of native cellulose. Structural rearrangements in nanosecond time scales were captured from the simulation set #2 that considered more than 20 separate simulations of 50 ns each. The ammonia−induced structural changes were monitored via three parameters: the distances a' and b' and the angle γ' (see the Supporting Information). At T = 298 K (see Figure 4, panels A and B), both a' and γ' evolve, over 10 ns, from their initial values typical of the cellulose I_β crystalline structure to values consistent with both the ammonia−cellulose I complex and cellulose III_I. Remarkably, no ammonia penetration is observed in any of the 10 ns trajectories at T = 298 K, confirming that early structural changes in our model fibril are mainly due to the effect of liquid ammonia as a bulk solvent surrounding the cellulose fibril. At T = 413 K, parameters a' and γ' reach a plateau value of ∼8.5 ± 0.4 Å and ∼114 ± 4°, respectively, both after ∼30−35 ns. Both of these crystalline parameters are consistent with a cellulose III_I structure. For the purpose of clarity, only the first 4 ns of the total 50 ns are shown in Figure 4, panels C and D. The crystal unit parameter b' (average value is 7.6 ± 0.4 Å for both T = 298 and 413 K), however, does not change during the global structural change. We do not observe a complete structural relaxation from I_β to III_I structure along the cellulose fibril main axis (direction perpendicular to the plane within which a', b', and γ' are calculated). Partial structural relaxation along the cellulose fibril main axis is observed only in the MD simulation at very high temperature (T = 650 K) suggesting that longer simulation times may be necessary to obtain the complete fibril structural relaxation.

The same set of simulations (#2) also provide microscopic details on the penetration of NH_3 molecules into cellulose fibril. Recent diffraction and MD simulation studies[9,10] were used to

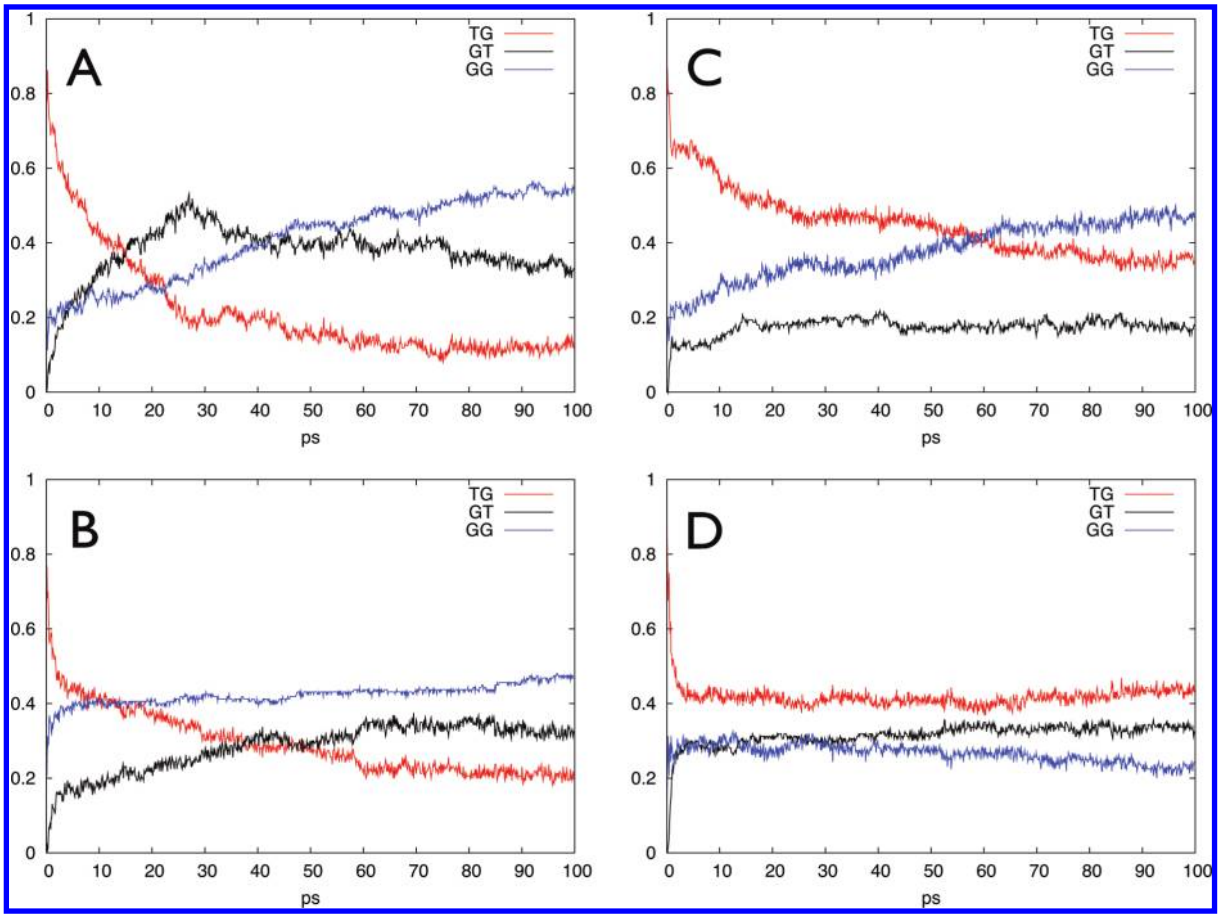

Figure 3. Representative plots of the early (100 ps) time evolution of the *tg*, *gt*, and *gg* fraction populations for solvent−exposed chains at T = 413 and 298 K (A and B, respectively) as well as for cellulose chains in the crystalline core at T = 413 and 298 K (C and D, respectively). The plots are generated from values averaged over 20 trajectories. The errors vary between 3% and 6%.

estimate the maximum (ideal) number of ammonia molecules (222) which can be "placed" into our model cellulose fibril. The time series for the ammonia penetration in Figure 4 monitor the fraction of this number. In terms of the fraction of ammonia molecules within the fibril (NH_3 fraction), the averaged data from the simulations at T = 413 K (Figure 4, panels C and D) show a much faster ammonia penetration with respect to the simulations at T = 298 K (Figure 4, panels A and B). In detail, the plots in Figure 4, panels C and D show a clear interplay between ammonia penetration and fibril structural changes, with partial relaxation for both a' and γ' (toward values compatible with the cellulose III_I structure) reached with very low ammonia penetration (NH_3 fraction ~0.2). The corresponding penetration of ammonia molecules occurs through the (100) and (−100) surfaces of the fibril.

In the new crystalline structure (see the bottom of Figure 1), the cellulose chains "sit" on top of each other forming stacks of cellulose molecules and "vertical channels" are created between the stacks. Our results suggest that the presence of these "channels" is necessary for the ammonia molecules to penetrate and eventually saturate the fibril. To confirm that, we ran an additional MD simulation (60 ns long) on a cellulose III_I fibril solvated with ammonia where the "vertical channels" between the stacks are present from the beginning of the simulation. Indeed, we observe that the ammonia penetration starts after a few simulation steps and proceeds rapidly to completely pervade the fibril (data not shown). It is also worth noting that, the penetration of the ammonia molecules does not seem to affect the structure of our model cellulose III_I fibril. The analysis of the ammonia penetration up to a time scale of 50 − 70 ns shows that, after a first rapid growth, the NH_3 fraction slowly increases up to ~0.35. Additional MD simulations at T = 450, 550, and 650 K qualitatively suggest that the rate of the ammonia penetration process monotonically increases with temperature. In particular, after 30 ns at T = 650 K, we observe that NH_3 fraction >99% and a quite distorted fibril loosely retaining a cellulose III_I structure (see Figure S5 in the Supporting Information).

The results presented in this computational study provide clues on improving the current lignocellulosic biomass chemical pretreatments such as liquid ammonia and ionic liquids (ILs) pretreatments[8,24] that rely on the disruption/alteration of the internal cellulose hydrogen bond network. First, our temperature dependent studies show that the liquid ammonia pretreatment should benefit from higher temperatures. This observation is consistent with a limited amount of information from the literature on liquid ammonia pretreatments[25,26] and the role of thermal cycling on cellulose crystallinity.[27,28] Importantly, we propose that the biggest gain at high temperature is seen in the eventual saturation of NH_3 molecules into the cellulose fibril. The early events associated with the perturbation of cellulose surface and the formation of channels can occur very rapidly even at low temperature. Therefore one does not need high

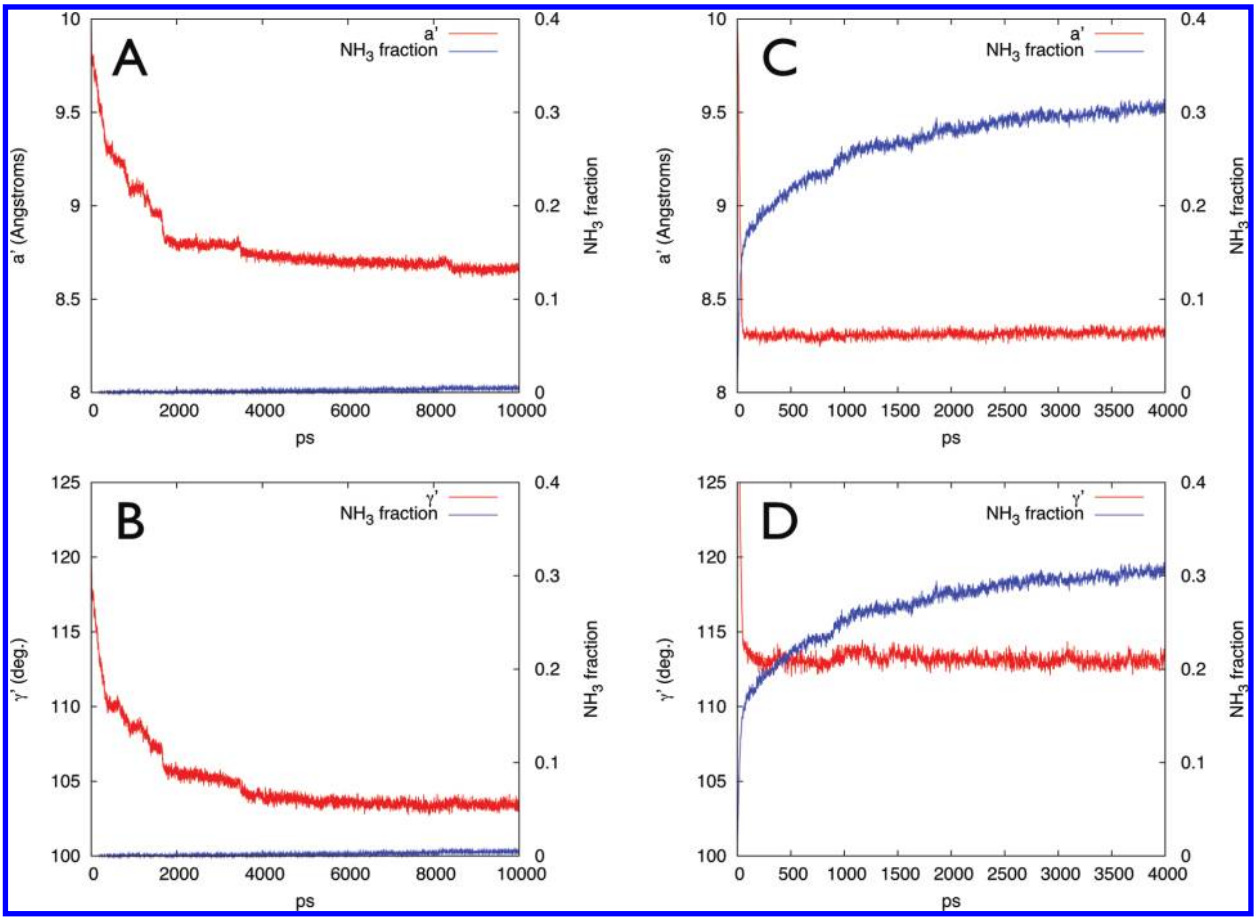

Figure 4. Time evolution for the structural parameters a', γ' and for the fraction of ammonia molecules within the cellulose fibril. (A and B) $T = 298$ K. a' and γ', respectively. (C and D) $T = 413$ K. a' and γ', respectively. The largest errors are 0.25 and 0.3 Å for a', at $T = 413$ and 298 K, respectively, and 3° and 12° for γ', at $T = 413$ and 298 K, respectively. For the fraction of NH_3 within the fibril the largest errors are 0.03 and 0.004 for a', at $T = 413$ and 298 K, respectively. The plots show data averaged over 10 different trajectories for both $T = 298$ and 413 K simulations.

temperatures to perturb the cellulose structure[29,30] as it can be done easily with bulk liquid ammonia at room temperature. One possible approach to improve existing ammonia−based pretreatments would be to use a gradient heating protocol to further decrystallize cellulose.

Finally, our study shows that the ability of a chemical species to strongly interact with the cellulose fibril surface appears to be, at least, as important as its ability to penetrate into the fibril. Therefore, experimental protocols can be further refined by choosing chemicals that show specificity to the hydrophobic (100) and (−100) fibril surfaces and at the same time exert enough chemistry to form an extended network of hydrogen bonds with the surface cellulose chains. With respect to ILs pretreatment, improvements may be obtained by tailor−making appropriate ILs that show high specificity for certain cellulose surfaces by polar anions without interference from the non polar cationic component (e.g., guanidium versus imidazolium or pyrimidium based cations).[31] Our studies imply that some of the inefficiencies in liquid ammonia treatment may arise due to inaccessibility of the (100) and (−100) surfaces. Indeed, the hydrophobic nature of these surfaces could facilitate lignin association and possibly impede cellulose accessibility to ammonia or ILs. One possible approach to improve the efficiency of liquid ammonia or ILs pretreatments will be to combine the pretreatments with carefully chosen organic solvents that can selectively extract lignin (and/or hemicellulose) from these surfaces and enable access to ammonia or ILs.

CONCLUSION

In summary, we provide a mechanistic model for early events in the liquid ammonia pretreatment of cellulosic biomass. The rapid formation of an extended hydrogen bond network between liquid ammonia and the cellulose molecules on the surface of the fibril induces a major shift in the hydroxymethyl group rotational state population. The change from *tg* to the *gt* and *gg* rotational states drives the structural crossover from cellulose I_β to a new crystalline structure compatible with both the ammonia−cellulose I complex and cellulose III_I. In the new crystalline structure, the cellulose chains stack on top of each other to form channels orthogonal to the (100) and (−100) surfaces of the fibril. These channels allow ammonia molecules to penetrate into the cellulose fibril. Such a mechanistic model with the proposed early microscopic events is consistent with X-ray time-resolved studies of EDA penetration into cellulose microfibrils from *Cladophora*,[32] thus suggesting that the mechanistic model deduced here for a small fibril can be applicable to larger fibrils as well. Finally, we have discussed possible ways in which the findings from the current studies can be incorporated into existing chemical pretreatments to make them more effective and economical.

■ ASSOCIATED CONTENT

Supporting Information. Additional figures referenced in the main manuscript. This material is available free of charge via the Internet at http://pubs.acs.org.

■ AUTHOR INFORMATION

Corresponding Author
*E-mail: gnana@lanl.gov.

Present Addresses
▽Oak Ridge National Laboratory, Oak Ridge, Tennessee 37831-6475, United States.

■ ACKNOWLEDGMENT

This work was funded by the LANL LDRD−X98U program and the computational resources were provided by LANL institutional computing. S.P.S.C. and B.E.D. thank the DOE Great Lakes Bioenergy Research Center (DOE BER Office of Science DE-FC02-07ER64494) for support

■ REFERENCES

(1) Ding, S.-Y.; Himmel, M. E. *J. Agric. Food Chem.* **2006**, *54*, 597–606.
(2) Himmel, M. E.; Ding, S.-Y.; Johnson, D. K.; Adney, W. S.; Nimlos, M. R.; Brady, J. W.; Foust, T. D. *Science* **2007**, *315*, 804–807.
(3) Binder, J. B.; Raines, R. T. *Proc. Natl. Acad. Sci. U.S.A.* **2010**, *107*, 4516–4521.
(4) Shen, T.; Gnanakaran, S. *Biophys. J.* **2009**, *96*, 3032–3040.
(5) Nishiyama, Y.; Langan, P.; Chanzy, H. *J. Am. Chem. Soc.* **2002**, *124*, 9074–9082.
(6) Wada, M.; Chanzy, H.; Nishiyama, Y.; Langan, P. *Macromolecules* **2004**, *37*, 8548–8555.
(7) Chundawat, S. P.; Bellesia, G.; Uppugundla, N.; da Costa Sousa, L.; Gao, D.; Cheh, A.; Agarwal, U. P.; Bianchetti, C. M.; Phillips, G. N. J.; Langan, P.; Balan, V.; Gnanakaran, S.; Dale, B. E. *J. Am. Chem. Soc.* **2011**, *133*, 11163−11174.
(8) Chundawat, S. P. S.; Beckham, G. T.; Himmel, M.; Dale, B. E. *Annu. Rev. Chem. Biomol. Eng.* **2011**, *2*, 121–145.
(9) Wada, M.; Nishiyama, Y.; Langan, P. *Macromolecules* **2006**, *39*, 2947–2952.
(10) Wada, M.; Nishiyama, Y.; Bellesia, G.; Forsyth, T.; Gnanakaran, S.; Langan, P. *Cellulose* **2011**, *18*, 191–206.
(11) Phillips, J.; Braun, R.; Wang, W.; Gumbart, J.; Tajkhorshid, E.; Villa, E.; Chipot, C.; Skeel, R.; Kale, L.; Schulten, K. *J. Comput. Chem.* **2005**, *26*, 1781–1802.
(12) Kirschner, K.; Yongye, A.; Tschampel, S.; González-Outeiriño, J.; Daniels, C.; Foley, L.; Woods, R. *J. Comput. Chem.* **2008**, *29*, 622–655.
(13) Case, D.; Cheatham, T.; Darden, T.; Gohike, H.; Luo, R.; Merz, K.; Onufriev, A.; Simmerling, C.; Wang, B.; Woods, R. *J. Comput. Chem.* **2005**, *26*, 1668–1688.
(14) Gao, J.; Xia, X.; George, T. F. *J. Phys. Chem.* **1993**, *97*, 9241–9247.
(15) Feller, S.; Zhang, Y.; Pastor, R.; Brooks, B. *J. Chem. Phys.* **1995**, *103*, 4613.
(16) Martyna, G. J.; Tobias, D. J.; L, K. M. *J. Chem. Phys.* **1994**, *101*, 4177.
(17) Darden, T.; York, D.; Pedersen, L. *J. Chem. Phys.* **1993**, *98*, 10089.
(18) Ryckaert, J.; Ciccotti, G.; Berendsen, H. *J. Comput. Phys.* **1977**, *23*, 327–341.
(19) Mills, J. E.; Dean, P. M. *J. Comput. Aided Mol. Des.* **1996**, *10*, 607–622.
(20) Luzar, A.; Chandler, D. *Nature* **1996**, *379*, 55–57.
(21) Reddy, C. K.; Das, A.; Jayaram, B. *J. Mol. Biol.* **2001**, *314*, 619–632.
(22) Mazeau, K.; Heux, L. *J. Phys. Chem. B* **2003**, *107*, 2394–2403.
(23) Shen, T.; Langan, P.; French, A. D.; Johnson, G. P.; Gnanakaran, S. *J. Am. Chem. Soc.* **2009**, *131*, 14786–14794.
(24) Liu, H.; Sale, K. L.; Holmes, B. M.; Simmons, B. A.; Seema, S. *J. Phys. Chem. B* **2010**, *114*, 4293–4301.
(25) Yatsu, L.; Calamari, T.; Benerito, R. *Text. Res. J.* **1986**, *56*, 419–424.
(26) Lewin, M.; Roldan, L. G. *J. Polym. Sci. Part C: Polym. Symp.* **1971**, *36*, 213–229.
(27) Cuculo, J.; Smith, C.; Sangwatanaroj, U.; Stejskal, E.; Sankar, S. *J. Polym. Sci. Part A: Polym. Chem.* **1994**, *32*, 229–239.
(28) Cuculo, J.; Smith, C.; Sangwatanaroj, U.; Stejskal, E.; Sankar, S. *J. Polym. Sci. Part A: Polym. Chem.* **1994**, *32*, 241–247.
(29) Wada, M. *J. Polym. Sci., Part B* **2002**, *40*, 1095–1102.
(30) Matthews, J.; Bergenstråhle, M.; Beckham, G. T.; Himmel, M.; Nimlos, M.; Brady, J.; Crowley, M. *J. Phys. Chem. B* **2011**, *115*, 2155–2166.
(31) Kahlen, J.; Masuch, K.; Leonhard, K. *Green Chem.* **2010**, *12*, 2172–2181.
(32) Nishiyama, Y.; Wada, M.; Hanson, B.; Langan, P. *Cellulose* **2010**, *17*, 735–745.